Journal of Sound and Vibration 568 (2024) 118056

Contents lists available at ScienceDirect

Journal of Sound and Vibration

journal homepage: www.elsevier.com/locate/jsvi

Acoustic scattering from spherical shells and its active control

Stephen Elliott *, Mihai Orita, Erika Quaranta, Jordan Cheer

Institute of Sound and Vibration Research, University of Southampton, United Kingdom

ARTICLE INFO

Keywords:
Acoustic scattering
Spherical shell
Spherical harmonics
Active control
Feedback control

ABSTRACT

The scattering of sound by a thin spherical shell is considered using an analytic formulation involving spherical harmonics. The integral of the far field scattered intensity, termed the scattered power, can then be expressed in a simple form. At low frequencies the scattered power can be minimised by an appropriate choice of material properties and shell thickness, which is illustrated for both a steel shell and for one in which the mass and stiffness of the shell are equal to those of the displaced fluid. Simulations of feedforward active control are then used to investigate the best possible performance in attenuating the scattered power, although this approach requires knowledge of the incident and scattered sound fields. Feedback control of the shell vibration using structural actuators and sensors is a more practical control strategy since it does not involve the need to separate the incident and scattered contributions. Direct velocity feedback control is considered using collocated and distributed actuators and sensors that spread the applied force and sensed velocity over spherical caps on the surface of the shell. This approach shows effective suppression of the structural shell modes that give rise to significant scattering at their resonant frequencies.

1. Introduction

The analysis of acoustic scattering is a classical problem in acoustics. Sound scattering is important in a number of applications, such as binaural sound reproduction, where the physical presence of the head plays an important role in the perceived sound [1], and in acoustic cloaking of objects [2,3] as in scenarios involving acoustic detection. The sound scattered from a body surrounded by a fluid can be calculated numerically, using finite elements or boundary elements for example, or analytically if the body has a simple shape, such as a sphere or cylinder [4,5].

More generally, Bobrovnitskii [6,7] introduced an impedance-based approach to the analysis of sound scattering from a body of arbitrary shape by assuming that the surface of the scattering body was divided into a large number of discrete elements, which are assumed to be small compared with a wavelength in the surrounding fluid. Assuming tonal excitation, the vectors of complex total pressures and total velocities at the positions of these discrete elements on the surface of the scattering body may be denoted as $\widetilde{\mathbf{p}}_t$ and $\widetilde{\mathbf{v}}_t$ respectively, where $\widetilde{\mathbf{v}}_t$ is measured normal and outward with respect to the surface and the tilde indicates that these quantities are evaluated at these discrete elements. Each of the vectors is made up of contributions from the sound field incident on the scattering body in the absence of the body, $\widetilde{\mathbf{p}}_i$ and $\widetilde{\mathbf{v}}_i$,and from the scattered acoustic field, $\widetilde{\mathbf{p}}_s$ and $\widetilde{\mathbf{v}}_s$, so that $\widetilde{\mathbf{p}}_t$can be written as $\widetilde{\mathbf{p}}_i$ plus $\widetilde{\mathbf{p}}_s$ and $\widetilde{\mathbf{v}}_t$ as $\widetilde{\mathbf{v}}_i$ plus $\widetilde{\mathbf{v}}_s$. Three input impedance matrices are then defined, which are the in-vacuo structural impedance matrix of the scattering body, $\widetilde{\mathbf{Z}}_B$, the impedance matrix of the internal volume of the scattering body if filled with the surrounding fluid, $\widetilde{\mathbf{Z}}_I$, and the outward

* Corresponding author.
E-mail address: sje@isvr.soton.ac.uk (S. Elliott).

https://doi.org/10.1016/j.jsv.2023.118056
Received 26 May 2023; Received in revised form 19 September 2023; Accepted 19 September 2023
Available online 20 September 2023

radiation impedance matrix on the surface of the scattering body into the surrounding fluid, $\widetilde{\mathbf{Z}}_R$, so that

$$\widetilde{\mathbf{p}}_t = -\widetilde{\mathbf{Z}}_B \, \widetilde{\mathbf{v}}_t, \tag{1}$$

$$\widetilde{\mathbf{p}}_i = -\widetilde{\mathbf{Z}}_I \, \widetilde{\mathbf{v}}_i, \tag{2}$$

$$\widetilde{\mathbf{p}}_s = \widetilde{\mathbf{Z}}_R \, \widetilde{\mathbf{v}}_s. \tag{3}$$

Using simple manipulations of the defining Eqs. (1)-(3), the vector of scattered surface pressures, $\widetilde{\mathbf{p}}_s$, can be expressed in terms of the vector of incident surface pressures, $\widetilde{\mathbf{p}}_i$, as [6,7]

$$\widetilde{\mathbf{p}}_s = \, (\widetilde{\mathbf{Y}}_R + \widetilde{\mathbf{Y}}_B)^{-1} (\widetilde{\mathbf{Y}}_I - \widetilde{\mathbf{Y}}_B) \, \widetilde{\mathbf{p}}_i, \tag{4}$$

where the admittance matrices $\widetilde{\mathbf{Y}}_B$, $\widetilde{\mathbf{Y}}_R$ and $\widetilde{\mathbf{Y}}_I$ are the inverses of the impedance matrices $\widetilde{\mathbf{Z}}_B$, $\widetilde{\mathbf{Z}}_R$ and $\widetilde{\mathbf{Z}}_I$, assuming that these matrices, and $\widetilde{\mathbf{Y}}_I - \widetilde{\mathbf{Y}}_B$, are non-singular. The scattered pressure is zero, as expected, if the admittance of the scattering body, $\widetilde{\mathbf{Y}}_B$, is equal to that of the fluid in the absence of the body, $\widetilde{\mathbf{Y}}_I$. The scattered pressure is also inversely dependant on the admittance of the shell when it is loaded by the fluid $\widetilde{\mathbf{Y}}_R + \widetilde{\mathbf{Y}}_B$. Under the conditions of linearity and reciprocity, these matrices are also symmetric, and when all the processes involved are passive, the real parts of the matrices are positive definite and so all of their associated impulse responses are causal. It is important to note that despite being formulated in terms of the in-vacuo structural response of the body, the loading of the fluid on the structure, as well as the sound scattering, are all accounted for in Eq. (4). Each of these impedance matrices is, in general, fully populated in this elemental formulation.

The vector of scattered pressures is defined on the surface of the scattering body, but it is also important to be able to calculate this pressure at other points in the fluid, particularly in the far field. This can generally be achieved using a radiation model in the fluid, but the formulation takes a simple form if we consider only the integral of the mean square scattered pressure over some surface in the far field, which may be termed the scattered power. It should be noted that this quantity does not represent the actual sound power radiated by the scattering object, but it is a normalised form of the scattering cross section.

If only the scattered field were present at the surface of the scattering object, the scattered power can be calculated from the surface pressure and surface velocity and in the elemental formulation would be equal to

$$\mathrm{W}_s = \frac{\Delta A}{2} Re \, \left[\widetilde{\mathbf{p}}_s^{\,\mathrm{H}} \, \widetilde{\mathbf{v}}_s \right] \tag{5}$$

Where *Re* denotes the real part of the term in brackets, the superscript H denotes the Hermitian transpose and for the sake of simplicity all the elements are assumed to have the same area, $\boldsymbol{\Delta A}$. Using the definition of $\widetilde{\mathbf{Y}}_R$, the scattered power can also be written as

$$\mathrm{W}_s = \frac{\Delta A}{2} \, \widetilde{\mathbf{p}}_s^{\,\mathrm{H}} \, Re \, [\widetilde{\mathbf{Y}}_R] \, \widetilde{\mathbf{p}}_s \tag{6}$$

which, using Eq. (4), can be calculated from only the incident field at the surface and the three impedance matrices defined in Eqs. (1)-(3).

This paper initially discusses a modal approach to Bobrovnitskii's theory of scattering, specifically for thin spherical shells. At low frequencies, when the size of the sphere is small compared with the acoustic wavelength in the surrounding fluid, the scattering is due to the rigid-body motion and the breathing mode of the shell and can be minimised by a suitable choice of shell thickness. If both the Young's modulus and the thickness of the shell can be controlled, then both of these two contributions to the low-frequency scattering can be cancelled, since the stiffness and mass of the shell can then be made equal to that of the displaced fluid. At higher frequencies the scattering is dominated by the fluid-loaded flexible modes of the shell, particularly due to ovalling, in which case the term $(\widetilde{\mathbf{Y}}_R + \widetilde{\mathbf{Y}}_B)$in Eq. (4) can become very small, giving rise to strong scattering. It is the cancellation of the reactive parts of these two acoustic admittances that causes strong scattering from bubbles at their resonant frequency, for example. It is shown, using a feedforward control formulation, how it is possible to greatly supress the scattering from these flexible modes using a small number of force actuators acting on the surface of the shell. The advantages of using structural actuators to modify the structural response, rather than using acoustic actuators to supress the scattered sound field, have been discussed, for example, by Eggler et al. [8]. Such a feedforward approach assumes separate knowledge of the incident and scattered sound fields, however, which complicates the practical implementation. Feedback control of the total velocity on the surface of the shell using force actuators is then discussed, which does not require separate knowledge of the incident and scattered sound fields. It is shown that for feedback control to be most effective on thin shells, the force actuators and velocity sensors must be distributed over a finite area of the sphere, so that they preferentially couple into the lower order flexible modes that contribute most to the scattering. Using velocity feedback with collocated actuators and sensors it is shown that good control can be achieved of the scattering from these flexible modes of the shell and that the scattered power can be attenuated so that it is below that of a rigid sphere. Initial versions of this work have been presented at two conferences [9,10], with some preliminary control results for the steel shell only and without the theory and discussion in Sections 3 and 5.

2. A modal approach for spherical shells

If instead of the vectors of total surface pressures and velocities being defined over a number of elements, they can be expressed in terms of some modal expansion, to give $\mathbf{p}_t$ and $\mathbf{v}_t$ for example, the scattering can be formulated using an entirely analogous definition of the matrices above, so that

$$\mathbf{p}_t = -\mathbf{Z}_B \ \mathbf{v}_t, \tag{7}$$

$$\mathbf{p}_i = -\mathbf{Z}_I \ \mathbf{v}_i, \tag{8}$$

$$\mathbf{p}_s = \mathbf{Z}_R \ \mathbf{v}_s, \tag{9}$$

where the lack of a tilde denotes the modal quantity. The vector of scattered surface pressures, $\mathbf{p}_s$, in this case can again be expressed in terms of the vector of incident surface pressures, $\mathbf{p}_i$, as [6,7]

$$\mathbf{p}_s = \ (\mathbf{Y}_R + \mathbf{Y}_B)^{-1}(\mathbf{Y}_I - \mathbf{Y}_B) \ \mathbf{p}_i = \mathbf{R} \ \mathbf{p}_i. \tag{10}$$

Any one of the impedance matrices above could be diagonalised by choosing a modal expansion involving either the structural modes of the body, for $\mathbf{Z}_B$, the interior acoustic modes of the space, for $\mathbf{Z}_I$, or the radiation modes, for $\mathbf{Z}_R$. The eigenvectors of any of the three impedance matrices could thus potentially be used to define this modal expansion. However, for the particular case of scattering from a thin uniform empty spherical shell in an infinite fluid, an expansion in terms of spherical harmonics diagonalises all three impedance matrices [7]. Rayleigh [4] first described how the scattered sound field from a rigid sphere could be obtained by satisfying the boundary conditions on the surface of the sphere using a form of spherical harmonic decomposition of the incident and scattered fields. The formulation has been extended, for example, by Godin [11], Mao et al., [12], and Elliott et al. [13] for the case of scattering from a locally reacting sphere.

The spherical harmonic expansions are truncated here to $n = N$ terms, so that the complex pressure and velocity distributions on the surface of the sphere can be expressed as

$$P(\theta,\varphi) = \sum_{n=0}^{N} \sum_{m=-n}^{n} p(n,m) \ Y_n^m(\theta,\varphi), \tag{11}$$

$$V(\theta,\varphi) = \sum_{n=0}^{N} \sum_{m=-n}^{n} v(n,m) Y_n^m(\theta,\varphi), \tag{12}$$

where $Y_n^m(\theta,\varphi)$ is the complex spherical harmonic of index (n,m) and $p(n,m)$ and $v(n,m)$denote the modal amplitudes of the surface pressure and velocity. In general the vectors of $(N+1)^2$ modal pressures and velocity amplitudes can then be defined as

$$\mathbf{p} = [p(0,0), \ p(1,-1), \ p(1,0), \ p(1,1)\ldots \ p(N,-N)\ldots \ p(N,0)\ldots \ p(N,N)]^T, \tag{13}$$

$$\mathbf{v} = [v(0,0), \ v(1,-1), \ v(1,0), \ v(1,1)\ldots \ v(N,-N)\ldots \ v(N,0)\ldots \ v(N,N)]^T. \tag{14}$$

The scattered sound power for the spherical harmonic expansion can be written as

$$\mathrm{W}_s = 2\pi a^2 \ Re \ \left[\mathbf{p}_s{}^{\mathrm{H}} \mathbf{v}_s\right] = 2\pi a^2 \ \mathbf{p}_s{}^{\mathrm{H}} Re \ [\mathbf{Y}_R] \ \mathbf{p}_s, \tag{15}$$

where a is the radius of the sphere. Assuming tonal excitation proportional to $e^{\mathrm{j}\omega t}$, the diagonal elements of the two acoustic impedance matrices, which are only dependant on the index n, can be written as [14]

$$Z_I(n) = \mathrm{j}\rho c \ \frac{j_n(ka)}{j_n'(ka)}, \tag{16}$$

$$Z_R(n) = -\mathrm{j}\rho c \ \frac{h_n(ka)}{h_n'(ka)}, \tag{17}$$

where ρ and c are the density and speed of sound in the surrounding fluid, $j_n(ka)$ and $h_n(ka)$ are the n-th order spherical Bessel function of the first kind and spherical Hankel function of the second kind and the prime superscript denotes derivation with respect to the nondimensional parameter, ka, where k is the acoustic wavenumber in the surrounding fluid. Since ka is equal to $2\pi fa\ /c$, where f is the frequency and c is a constant, because the surrounding fluid is not dispersive, this parameter represents the normalised frequency.

The in-vacuo modal impedance of a thin uniform empty spherical shell is also only dependant on n and is given by [5]

$$Z_B(n) = j\frac{\rho_s c_p}{\Omega} \frac{h}{a} \frac{\left(\Omega^2 - \Omega_{n1}^2\right)\left(\Omega^2 - \Omega_{n2}^2\right)}{\Omega^2 - \left(1+\beta^2\right)(\nu + \lambda_n - 1)}, \tag{18}$$

where ρ_s is the density of the shell, $c_p^2 = E/[\rho_s(1-\nu^2)]$ with E and ν being the Young`s modulus and Poisson`s ratio of the shell, h is the

shell thickness, β^2 is $h^2/(12a^2)$, λ_n is $n(n+1)$, and Ω is $\omega a/c_p$ with $\omega = kc$, which can also be written as $\Omega = (c/c_p)ka$. The values of Ω_{n1} and Ω_{n2} are the in-vacuo natural frequencies of vibration of the shell and are given by the solutions to the equation

$$\Omega^4 - \left[1 + 3\nu + \lambda_n - \beta^2\left(1 - \nu - \lambda_n^2 - \nu\lambda_n\right)\right]\Omega^2 + (\lambda_n - 2)\left(1 - \nu^2\right) + \beta^2\left[\lambda_n^3 - 4\lambda_n^2 + \lambda_n\left(5 - \nu^2\right) - 2\left(1 - \nu^2\right)\right] = 0, \tag{19}$$

although there is only one real natural frequency for $n = 0$, corresponding to the breathing mode, and for the $n = 1$ mode one of the natural frequencies is zero, corresponding to the shell moving to and fro as a rigid body [15]. It is convenient to write the in-vacuo impedance of the shell normalized by the characteristic acoustic impedance of the fluid, ρc, as

$$\zeta_n(ka) = Z_B(n)/\rho c, \tag{20}$$

where $Z_B(n)$ in Eq. (18) is implicitly a function of ka.

In this study we initially assume that the incident sound wave is propagating along the z axis, from z equals infinity, and so only excites the spherical harmonics for which $m = 0$. Similarly all secondary excitations of the shell will initially be assumed to be axisymmetric, so that the vectors defined in Eqs. (13) and (14) can be considerably simplified so that they contain only $N+1$ terms, for $n = 0$ to N. The diagonal elements of the admittance matrices in Eq. (10), which are the reciprocal of the impedancesin Eqs. (16), (17) and Eq. (18), can be written as $Y_B(n)$, $Y_R(n)$ and $Y_I(n)$. The scattered pressure for the n-th mode, $p_s(n)$, depends only on the n-th mode of the incident pressure, $p_i(n)$, and their ratio can be written

$$\frac{p_s(n)}{p_i(n)} = \frac{Y_I(n) - Y_B(n)}{Y_R(n) + Y_B(n)} = -\frac{h_n(ka)}{j_n(ka)}\frac{j_n(ka) + j\zeta_n(ka)j_n'(ka)}{h_n(ka) + j\zeta_n(ka)h_n'(ka)} . \tag{21}$$

For a plane incident wave the n,m-th mode of the incident pressure is given in the general case by [14]

$$p_i(n,m) = (\mathrm{j})^n 4\pi P_i\, j_n(ka)\overline{Y_n^m}(\theta_i, \varphi_i) \tag{22}$$

where P_i is the complex amplitude of the incident pressure, the plane wave is incident from the direction θ_i, φ_i and the overbar denotes complex conjugation. In the particular case of axisymmetric excitation, then θ_i is either zero or π, and the expression is only finite for $m = 0$ so that Eq. (22) can just be written as $p_i(n)$. The acoustic power associated with the incident plane wave, W_i, can be defined to be the product of the incident intensity and the cross-sectional area of the sphere, so that

$$\mathrm{W}_i = \frac{\pi a^2}{2\rho c}|P_i|^2. \tag{23}$$

Using Eqs. (21) and (22) in (15), the normalised scattered power of a spherical shell in response to an axisymmetric incident plane-wave can be written as,

$$\Pi_s = \frac{W_s}{W_i} = \frac{4}{(ka)^2}\sum_{n=0}^{N}(2n+1)\left|A_n^s\right|^2, \tag{24}$$

where

$$A_n^s = \frac{j_n(ka) + j\zeta_n(ka)j_n'(ka)}{h_n(ka) + j\zeta_n(ka)h_n'(ka)}. \tag{25}$$

This equation is a generalisation of the result in [13] for a locally reacting sphere, in which the normalised modal impedance of the scattering shell now depends on both the modal index, n, and on the normalised frequency, ka.

3. Minimising the low frequency scattering by shell design

At very low frequencies, the modal coefficients in Eq. (25) can be calculated by taking the limit of $ka \ll 1$ for the various terms [16]. For the $n = 0$ and $n = 1$ terms, this gives

$$\lim_{ka\ll 1} A_0^s = -j\frac{(ka)^3}{3}\left(1 - \frac{3\rho c^2(1-\nu)}{2E}\frac{a}{h}\right), \tag{26}$$

$$\lim_{ka\ll 1} A_1^s = j\frac{(ka)^3}{3}\left(\frac{3\frac{h}{a}\frac{\rho_s}{\rho} - 1}{1 + 6\frac{h}{a}\frac{\rho_s}{\rho}}\right). \tag{27}$$

It is possible to set the low frequency limit for A_0^s to zero if the normalised shell thickness is given by

$$\frac{h}{a} = \frac{3\rho c^2(1-\nu)}{2E}, \tag{28}$$

which corresponds to the compressional stiffness of the shell being equal to that of the displaced fluid. It is also possible to set the low

frequency limit for A_1^s to zero if the normalised thickness of the shell is given by

$$\frac{h}{a} = \frac{\rho}{3\rho_s}, \tag{29}$$

which corresponds to the condition that the mass of the shell is equal to that of the displaced fluid, i.e. the shell is neutrally buoyant. These conditions are similar to those discussed in [17,18] for a shell surrounded by a soft coating, and such an arrangement has been demonstrated to reduce the scattering from coated cylinders in practice [19].

The two conditions for the shell thickness, (28) and (29), are simultaneously satisfied if the properties of the shell satisfy the following condition

$$\frac{2E}{9(1-\nu)\rho_s} = c^2. \tag{30}$$

More generally, the low frequency normalised scattered power can be obtained by just considering the first two terms in Eq. (24), which can be written using Eqs. (26) and (27), as

$$\lim_{ka\ll 1}\Pi_s = \frac{4(ka)^4}{9}\left\{\left(1-\frac{3\rho c^2(1-\nu)}{2E}\frac{a}{h}\right)^2 + 3\left(\frac{3\frac{h}{a}\frac{\rho_s}{\rho}-1}{1+6\frac{h}{a}\frac{\rho_s}{\rho}}\right)^2\right\}. \tag{31}$$

At low frequencies, the normalised scattered power for a rigid sphere that is fixed in space, $\lim_{ka\ll 1}\Pi_{sR}$, is given by

$$\lim_{ka\ll 1}\Pi_{sR} = \frac{7(ka)^4}{9}. \tag{32}$$

Where Lamb [20] showed that 4/9 of this is due to the sphere being incompressible, which Eq. (31) limits to if E is very large and $h/a = \rho/(3\rho_s)$ and that 3/9 of this is due to it not being able to move as a rigid body, which this equation limits to if ρ_s is very large and $h/a = 3\rho c^2(1-\nu)/(2E)$. The low frequency limit for the scattered power of a spherical shell, normalised by that of a rigid sphere is thus

$$\lim_{ka\ll 1}\left[\frac{\Pi_s}{\Pi_{sR}}\right] = \frac{4}{7}\left\{\left(1-\frac{3\rho c^2(1-\nu)}{2E}\frac{a}{h}\right)^2 + 3\left(\frac{3\frac{h}{a}\frac{\rho_s}{\rho}-1}{1+6\frac{h}{a}\frac{\rho_s}{\rho}}\right)^2\right\}, \tag{33}$$

This is plotted as a function of the shell thickness in Fig. 1 for a steel shell and for an "alloy" shell in water. The density of the alloy shell is assumed to be 10,000 kg/m^3 and its Young's modulus is chosen so that Eq. (30) is satisfied, assuming that the Poisson's ratio is the same as that of steel, as listed in Table 1. The density of the alloy is thus slightly greater than steel and it is assumed that its Young's modulus can be altered using a combination of materials and/or thermal treatment to reach the required value. The normalised scattered power in Fig. 1 goes to zero for the alloy shell when the thickness satisfies Eqs. (28) and (29), so that h/a is 1/30 in this case. This condition is not too sensitive however, since the scattered power only rises to be one tenth of that for the rigid sphere if the shell thickness changes from its optimum value by about 12% or if the speed of sound in the fluid changes by about 6%. The steel shell also has a minimum in the low frequency scattered power plotted in Fig. 1, when h/a is about 2.31%, although its scattered power is then

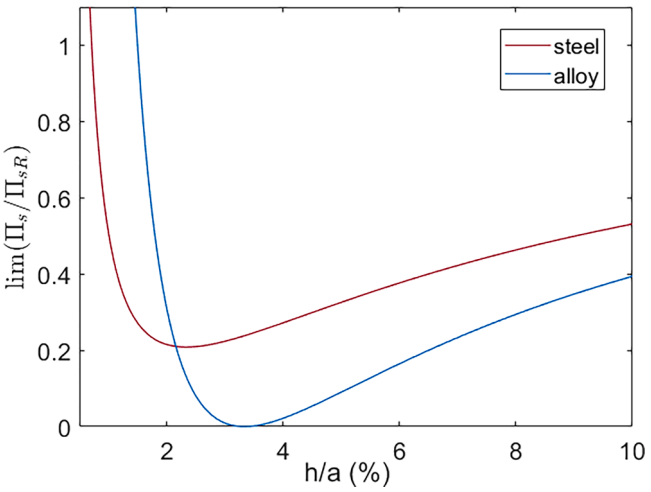

Fig. 1. The low frequency limit of the scattered power, for a steel shell and for an alloy shell in water, normalised by the scattered power of a rigid sphere, as a function of the normalised shell thickness.

Table 1
Material properties of the two shells, which are assumed to be immersed in water with a density of 1,000 kg/m^3 and a speed of sound of 1,500 m/s.

Shell	E (GPa)	ρ_S (kg/m^3)	ν	h/a (%)
Steel	195	7700	0.28	2.31
Alloy	72.9	10,000	0.28	3.33

still finite, and about 0.23 times that scattered by a rigid sphere.

Fig. 2 shows the normalised scattered power as a function of the normalised frequency ka resulting from a single incident plane wave in water for the steel and alloy shells, whose properties and thicknesses are given in Table 1. The limit in the modal summation, N, in Eq. (24) was taken to be 100 for these simulations up to $ka = 100$, although it was found that the scattered power did not change by more than 0.06 dB if N was doubled. It can be seen that at low frequencies, below about $ka = 0.9$, the scattered power from the alloy shell is significantly smaller than that from the steel shell.

The first peak in the scattered power for both shells in Fig. 2 is due to an $n = 2$, ovalling [15], structural mode of the loaded shell, which occurs for a value of ka of about 1.0 for the alloy shell and about 1.4 for the steel shell. This peak in the scattered power for the alloy shell is sharper than that for the steel shell, since the damping of this mode due to sound radiation is considerably greater for the steel shell. This is illustrated in Fig. 3, which shows the real and imaginary parts of the normalised radiation impedance for the $n = 2$ spherical harmonic in Eq. (17). The real part of this impedance, which will add damping to the response of the shell, is much smaller at $ka = 1.0$, corresponding to the resonance of the alloy shell, than it is at $ka = 1.4$, corresponding to the resonance of the steel shell. The imaginary part of the radiation impedance adds mass loading to the shell and so lowers its resonance frequency compared to the in-vacuo resonance frequencies given by the solutions to Eq. (19) [5]. For example, the first natural frequency for the $n = 2$ mode of the alloy shell has a normalised frequency of about $ka = 1.3$ in vacuo, whereas this is reduced by fluid loading to be about $ka = 1.0$. Even if some material damping is added to the shells, by including a small imaginary component of 1% in the Young's modulus, the first peak in the scattering for the alloy shell is still more lightly damped than that of the steel shell, as also shown in Fig. 2. This amount of material damping does, however, more effectively attenuate the very lightly damped resonances at about $ka = 1.2$ and 1.4 for the alloy shell, which are due to its fluid-loaded $n = 3$ and $n = 4$ structural modes. Most engineering structures will have a loss factor of at least 1% and so this level of structural damping is retained in the following simulations.

To reinforce the discussion above, Fig. 4 shows the contributions to the total scattered power from the first few structural modes of the two shells. Also shown, for comparison, is the power scattered by a rigid sphere that is fixed in space. The low frequency behaviour for the steel shell follows the same power law as the rigid sphere, being proportional to $(ka)^4$, but is lower by a factor of about 0.23, as predicted in Fig. 1. The $n = 0$ and $n = 1$ contributions are much less for the alloy shell, as expected, which follows a power law of $(ka)^8$ at very low frequencies [16] and so is much reduced compared to the rigid sphere. Somewhat above the frequency of the $n = 2$ structural resonance, the overall scattering from the steel shell is about double that of the rigid sphere, for ka from about 2 to 5, whereas that for the alloy shell is less than half that of a rigid sphere, for ka from about 1.5 to 3. For the steel shell, this is because there

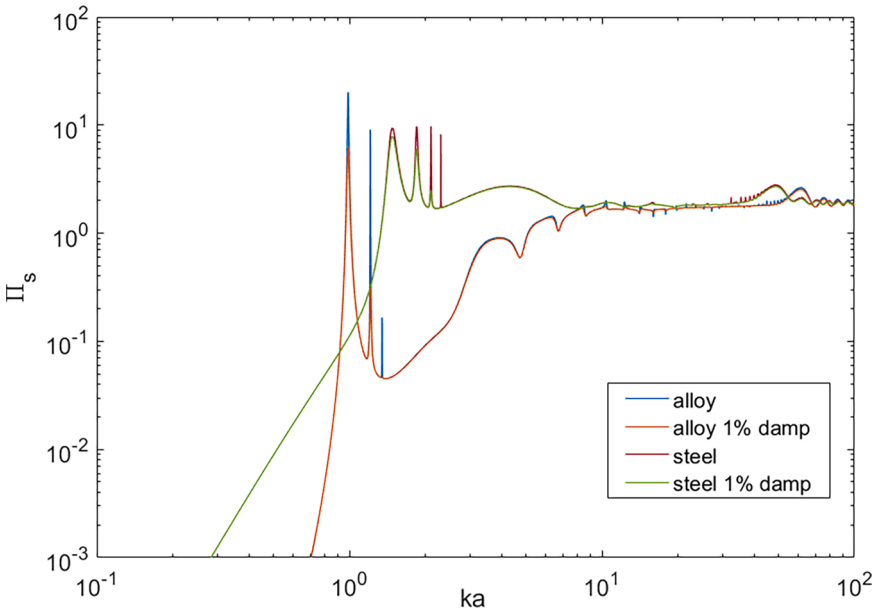

Fig. 2. The normalised scattered power, as a function of normalised frequency, for the steel and the alloy shells, whose material properties and thicknesses are shown in Table 1, in water, both without any material damping and with 1% damping loss factor.

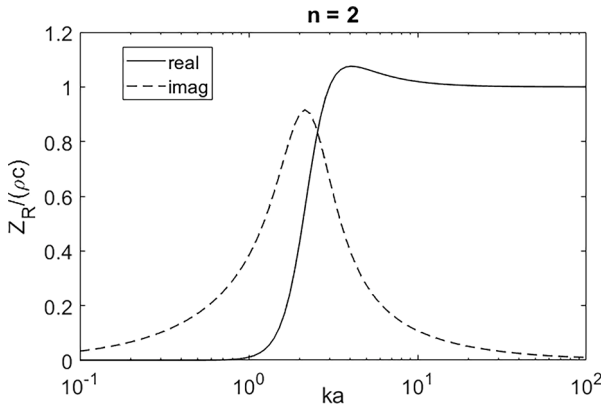

Fig. 3. The real and imaginary parts of the normalised acoustic radiation impedance for the $n = 2$ spherical harmonic.

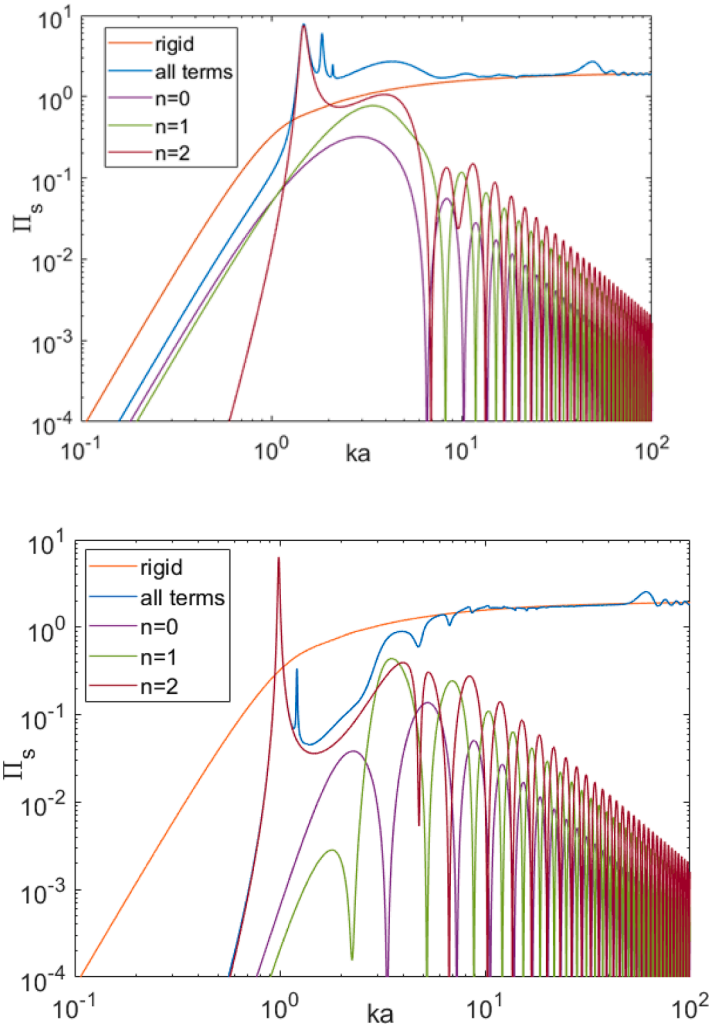

Fig. 4. Overall normalised scattered power from the steel, (upper) and alloy, (lower), shells and the individual components due to the $n = 0$, $n = 1$ and $n = 2$ structural modes. Also shown is the normalised scattered power for a rigid sphere that is fixed in space.

are significant contributions from the $n = 0$, $n = 1$ and $n = 2$ structural modes in this frequency region. For the alloy shell, however, the contributions from the $n = 0$ and $n = 1$ structural modes are still small in this frequency region, giving a dip in the scattered power that is significantly below that of the rigid sphere.

4. Active feedforward control of tonal incident fields

If the incident field is tonal and of known frequency, a frequency-domain feedforward control formulation can be used to calculate the optimal performance of an array of secondary sources in minimising the scattered power, assuming knowledge of the incident and scattered fields [21]. A frequency domain approach allows evaluation of the best possible performance of an active system with a given number of secondary sources, without having to be concerned with the sensing of the reference or of the error signals, or with the implementation of a causal controller. It can thus be used as the first step in a hierarchical design approach for active control [22].

In the general case the shell is assumed to be controlled with L internal and outward-facing active point forces, with an individual magnitude of f_l, positioned at (θ_l, φ_l), that generates a modal pressure acting on the shell of [5]

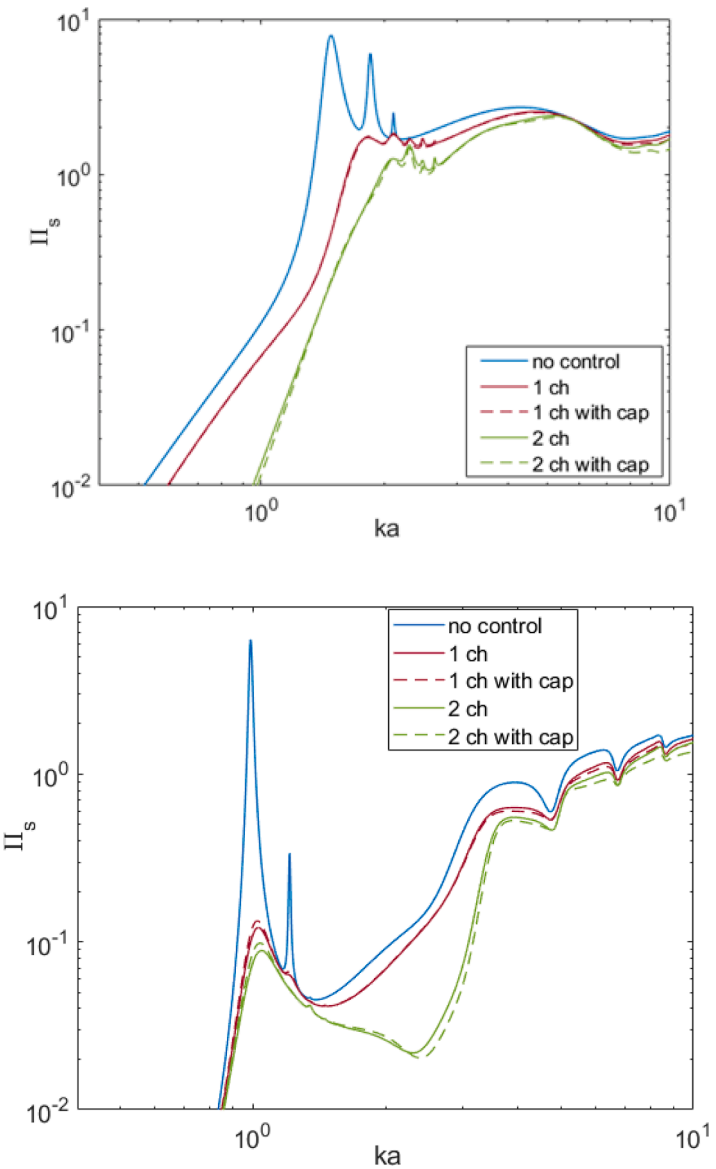

Fig. 5. Optimal results of using active feedforward control with one or two internal point force actuators to minimise the scattering from the steel (upper) or alloy (lower) shell in water. Also shown are the results of feedforward control with spherical cap actuators, as used in Section 5.

$$p_l(n,m) = -\left[\frac{Z_B(n)}{Z_B(n)+Z_R(n)}\right] \frac{f_l}{a^2}\overline{Y}_n^m(\theta_l,\varphi_l), \tag{34}$$

where the overbar again denotes complex conjugation. The scattered modal pressure after control with L secondary point-forces is thus

$$p_{sc}(n,m) = p_s(n,m) - \left[\frac{Z_B(n)}{Z_B(n)+Z_R(n)}\right] \sum_{l=1}^{L} \frac{f_l}{a^2}\overline{Y}_n^m(\theta_l,\varphi_l), \tag{35}$$

which can be written in vector form as

$$\mathbf{p}_{sc} = \mathbf{p}_s - \mathbf{B}\,\tilde{\mathbf{p}}_c, \tag{36}$$

where $\tilde{\mathbf{p}}_c = \frac{1}{a^2}[f_1,\ f_2,\ f_3 \ldots f_L]^T$ is the vector of L normalised control forces, which has a tilde to denote that these are discrete rather than modal pressures. The matrix $\mathbf{B}$ is equal to $\mathbf{Z}_B[\mathbf{Z}_B+\mathbf{Z}_R]^{-1}$ times the matrix $\mathbf{S}$, for which in general the l-th column has elements of the form $\overline{Y}_n^m(\theta_l,\varphi_l)$, although in the axisymmetric case we only consider terms with $m=0$ and so the matrix has dimensions $N+1$ by L.

The scattered power after control is given by a modified form of Eq. (15),

$$W_{sc} = 2\pi a^2\ \mathrm{Re}\{\mathbf{p}_{sc}^{\mathrm{H}}\mathbf{v}_{sc}\} = 2\pi a^2\ \mathbf{p}_{sc}^{\mathrm{H}}\mathrm{Re}\{\mathbf{Y}_R\}\mathbf{p}_{sc}, \tag{37}$$

which is a quadratic function of $\tilde{\mathbf{p}}_c$. The scattered pressure can thus be minimised by the vector of control forces, as derived in Appendix A, given by

$$\tilde{\mathbf{p}}_c^{(\mathrm{opt})} = \left[\mathbf{B}^{\mathrm{H}}\mathrm{Re}\{\mathbf{Y}_R\}\mathbf{B}\right]^{-1}\mathbf{B}^{\mathrm{H}}\mathrm{Re}\{\mathbf{Y}_R\}\mathbf{R}\ \mathbf{p}_i, \tag{38}$$

where Eq. (10) has been used to relate $\mathbf{p}_s$ to $\mathbf{p}_i$.

Fig. 5 shows the results of minimising the scattered sound power of the steel and alloy shell described above, using either a single point secondary force, facing the incident wave, or two point secondary forces, facing towards and away from the incident wave. The frequency range has been enlarged compared to Fig. 2, for clarity. For the steel shell, significant control of the scattered sound power can be achieved at frequencies below about $ka = 2$, particularly at the resonant frequencies of the shell and with two secondary forces. At very low frequencies and with two secondary forces this is achieved by actively attenuating both the $n=0$ and $n=1$ structural modes, which correspond to compression of the shell and rigid body translation. This requires much larger magnitudes of secondary forces than those required to control the resonant structural modes at higher frequencies, however [16]. These results are in general agreement with those presented by Avital and Miloh [23] for the case of feedforward control with a single secondary force. For the alloy shell, only limited reductions are achieved at very low frequencies, since the contributions of the $n=0$ and $n=1$ structural modes to the scattered power have already been significantly reduced by passive design, as seen in Fig. 4. Feedforward control is very effective at reducing the scattered power due to the resonances of the higher order structural modes for the alloy shell, however. For completeness, Fig. 5 also shows the performance of the feedforward control system with two distributed force actuators, corresponding to spherical caps on the poles of the sphere, calculated using a modification of the $\mathbf{S}$ matrix described in the following Section. The results with the spherical cap actuators are very similar to those with the point force actuators in the feedforward case, since at any single frequency the shell response is dominated by only a few modes and so the control forces can be adjusted one frequency at a time to attenuate these modes, without the resulting excitation of the higher order modes causing undue additional sound radiation.

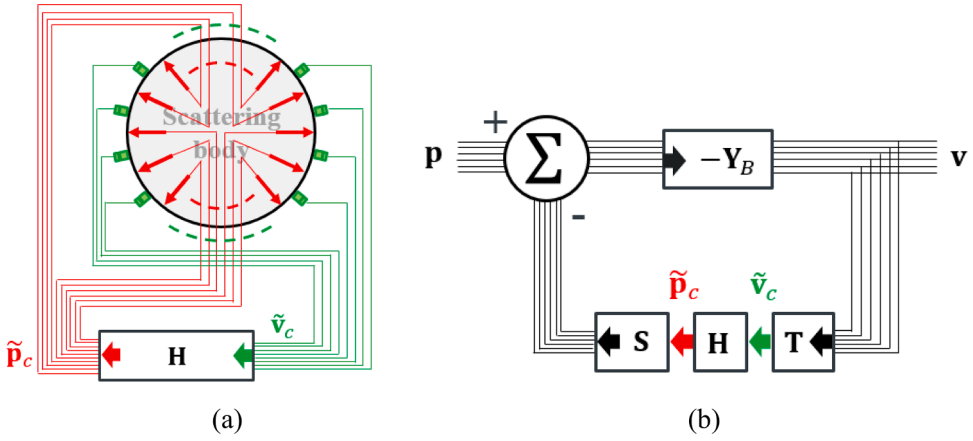

Fig. 6. Feedback control using secondary force actuators driven by the measured velocities at discrete sensors on the surface of the body (a), and the block diagram of the equivalent modal feedback system (b).

5. Direct velocity feedback control

The effect of active feedback control on scattering can be calculated by initially considering the consequences of feedback control on the in-vacuo response of the shell. Fig. 6(a) shows the general physical arrangement in which the signals from K discrete velocity sensors are fed to L internal force actuators via a feedback controller matrix, $\mathbf{H}$. A block diagram showing the effect of such a controller on the modal velocity of the shell, in response to a general modal pressure excitation, is also shown in Fig. 6(b).

In the absence of control, the vector of overall modal velocities on the shell, $\mathbf{v}$, in response to a general vector of overall modal pressures, $\mathbf{p}$, is given, using Eq. (7), by

$$\mathbf{v} = -\mathbf{Y}_B \, \mathbf{p} \, . \tag{39}$$

In the presence of active control with an array of internal forces, as in Section 4, the modal pressures acting on the shell are modified, although in this in-vacuo case there is no fluid loading and the matrix $\mathbf{B}$ in Eq. (36) reduces to $\mathbf{S}$, so that

$$\mathbf{v} = -\mathbf{Y}_B(\mathbf{p} - \mathbf{S} \, \widetilde{\mathbf{p}}_c). \tag{40}$$

For the feedback arrangement shown in Fig. 6(a), the secondary forces are due to feedback from the velocities at the sensor positions, $\widetilde{\mathbf{v}}_c$, which also has a tilde to denote discrete rather than modal velocities, via the feedback control matrix $\mathbf{H}$, so that

$$\widetilde{\mathbf{p}}_c = \mathbf{H} \, \widetilde{\mathbf{v}}_c, \tag{41}$$

where

$$\widetilde{\mathbf{v}}_c = \mathbf{T} \, \mathbf{v}, \tag{42}$$

$\mathbf{v}$ being the vector of modal velocities, and $\mathbf{T}$ is a coupling matrix, of dimensions K by $N + 1$ in the axisymmetric case since we only consider terms with $m = 0$, although in the general case, from Eq. (12), it has elements of the form $Y_n^m(\theta_k, \varphi_k)$. The vector of modal velocities can thus be written as,

$$\mathbf{v} = -\mathbf{Y}_B(\, \mathbf{p} - \mathbf{SHT} \, \mathbf{v}), \tag{43}$$

and so,

$$\mathbf{v} = -[\mathbf{I} + \mathbf{Y}_B\mathbf{SHT}]^{-1}\mathbf{Y}_B\mathbf{p} \, . \tag{44}$$

The vector of modal pressures can thus be expressed as

$$\mathbf{p} = -\mathbf{Z}_B[\mathbf{I} + \mathbf{Y}_B\mathbf{SHT}]\mathbf{v} = -\mathbf{Z}_B^{(cl)}\mathbf{v}, \tag{45}$$

where $\mathbf{Z}_B^{(cl)}$ is the overall modal impedance for the shell with closed-loop feedback control, which can be written as

$$\mathbf{Z}_B^{(cl)} = \mathbf{Z}_B + \mathbf{SHT} \, . \tag{46}$$

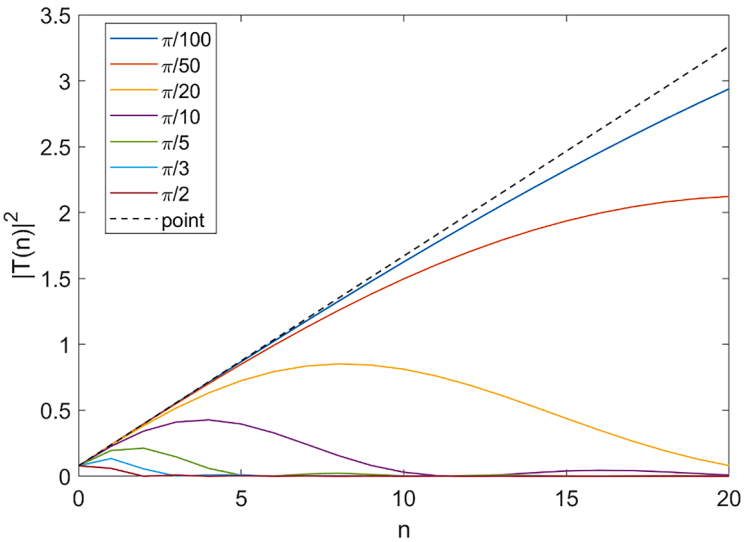

Fig. 7. The modulus squared coupling coefficient, $|\mathbf{T}(\boldsymbol{n})|^2$, for a spherical cap actuator and sensor coupling into the structural modes of a spherical shell as a function of the order of the structural mode. This is plotted for various spherical cap angles, $\boldsymbol{\theta}_0$, and also for a point force and point velocity sensor, dashed line.

Although the modal structural impedance matrix $\mathbf{Z}_B$ is diagonal for a uniform spherical shell, the modifying impedance matrix due to feedback control, **SHT**, is not diagonal in general. Nevertheless, the fully-populated matrix $[\mathbf{Z}_B^{(cl)}]^{-1}$ can now be used instead of $\mathbf{Y}_B$ in Eq. (10) to calculate the vector of scattered modal pressures after feedback control in terms of the vector of incident modal pressures, and, hence, the scattered power after control can again be calculated using Eq. (15).

Several designs of feedback controller are possible. The simplest is decentralised local velocity feedback using collocated actuators and sensors, for which **H** is equal to $\gamma\mathbf{I}$, where γ is the gain of each local feedback loop. In this collocated case, the coupling matrix for the actuators, **S**, is equal to the Hermitian transpose of the coupling matrix for the sensors, $\mathbf{T}^{\mathrm{H}}$, and the control system is unconditionally stable for positive values of γ . Unfortunately, this simple control strategy is not very successful with point force actuators and point velocity sensors, since this combination preferentially couples into and attenuates the higher order structural modes, rather than the lower order structural modes that need controlling. This is illustrated in Fig. 7, which shows, as a function of the mode order n, the squared magnitude of the n-th element of the coupling matrix, **T** in Eq. (42), for a single actuator/sensor pair, $|\mathrm{T}(n)|^2$, which is proportional to the diagonal terms in the matrix **SHT** in this collocated case. For point force actuators and velocity sensors, the magnitude of these terms continues to grow with n, since in this case $|\mathrm{T}(n)|^2$ is given by $|Y_n^0(0,0)|^2$, which equals $(2n+1)/4\pi$.

This problem can be overcome if spatially distributed force actuators and velocity sensors are used, which couple less efficiently into the higher order modes. The output of a spherical cap sensor centred on $\theta = \theta_k,\ \varphi = \varphi_k$, for example, can be calculated by integrating the velocity of the shell over a finite polar angle of $\pm\,\theta_0$, as discussed in Appendix B, for which the elements of the coupling matrix, **T**, in the general case of Eq. (42), then take the form

$$\mathrm{T}(n,m) = \left[\frac{P_{n-1}(\cos\,\theta_0) \;-\; P_{n+1}(\cos\,\theta_0)}{(2n+1)(1-\cos\,\theta_0)}\right] Y_n^m(\,\theta_k,\ \varphi_k), \tag{47}$$

where $\mathrm{P}_n(\cos\,\theta_0)$ is the n-th order Legendre polynomial and $\mathrm{P}_{-1}(\cos\,\theta_0) = 1$. The same additional term, in square brackets, also appears in the elements of the matrix, **S**, that describes the structural coupling of a spherical cap force actuator into the modal force on the shell, which is a similar problem to the analysis of the sound field from a circular piston in a spherical baffle [5,14]. Fig. 7 shows the magnitude of $|\mathrm{T}(n)|^2$ for this combination of spherical cap actuator and sensor, for various spherical cap angles, θ_0 . In this case the coupling falls off as n increases, with a greater rate of fall-off as θ_0 gets larger. For $\theta_0 = \pi/100$, the coupling is similar to a point actuator and sensor up to about $n = 10$, but for $\theta_0 = \pi/10$ the response starts to fall off after about $n = 4$, so that the diagonal terms in the matrix **SHT** now become smaller for larger values of n. This combination of actuator and sensor thus couple into the structural modes of the shell that scatter most effectively, rather than the much higher order modes that do not. Fig. 8 illustrates the physical arrangements for control with this form of distributed actuator and sensor, and for an arrangement with one or two such actuator and sensor pairs.

The direct velocity feedback gain, γ, can be chosen to give a reasonable compromise between supressing the original lightly damped structural resonances and not exciting higher-order resonances by pinning the structure [24,25]. Fig. 9 shows the maximum value of the normalised scattered power for the two shells around the $n = 2$ resonance, as a function of the normalised feedback gain for both single and two channel decentralised direct velocity feedback controllers and for both the steel and alloy shells with spherical cap actuators and sensors. It can be seen that this response is minimised in all cases if the normalised feedback gain is set to a value of about 0.2.

Fig. 10 shows the effect of decentralised velocity feedback, using this value of normalised feedback gain, on the scattered power from the steel and the alloy shells with one or two spherical cap force actuators and collocated velocity sensors. In this case the more general matrix formulation for the scattered power given by Eq. (15) must be used, rather than the simplification in Eq. (24) used above, since the matrix $\mathbf{Y}_B$ is no longer diagonal. The feedback controller is able to attenuate the vibration of the $n = 2$ resonance in

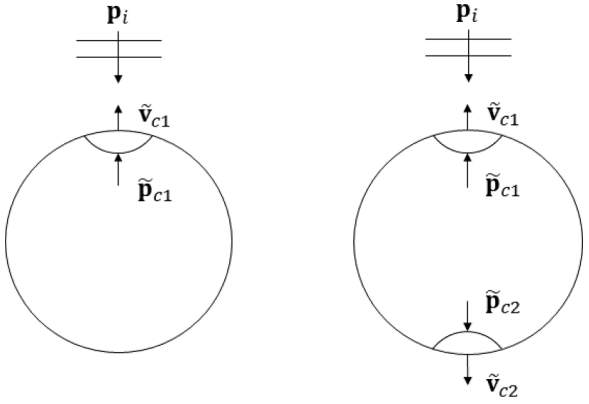

Fig. 8. Arrangements in which a spherical cap actuator is driven by the normalised secondary force, $\tilde{\mathbf{p}}_c$, and the output of a distributed velocity sensor is given by $\tilde{\mathbf{v}}_c$ for use in a collocated feedback control, in the case of a single channel system, left, a two channel system, right, both with incident waves along the z axis.

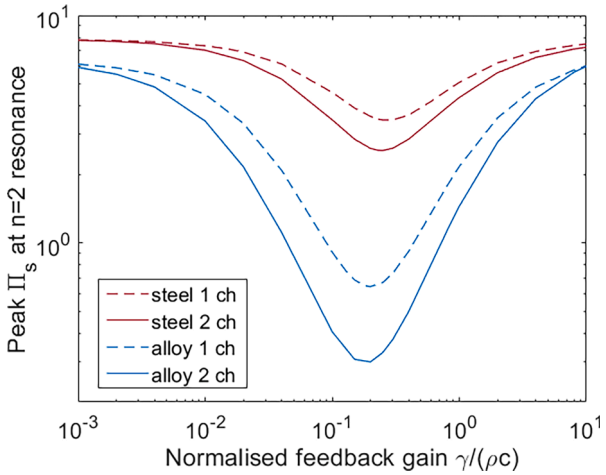

Fig. 9. The peak value of the normalised scattered power around the $n = 2$ resonance for both the steel and the alloy shell as a function of the normalised feedback gain, for direct velocity feedback control systems using spherical cap force actuators and collocated velocity sensors, with $\theta_0 = \pi/10$, and either one or two channel decentralised systems.

both cases, and with two actuator/sensor pairs reduces the scattered power at this resonance frequency, by about 5 dB in the case of the steel shell and by about 13 dB in the case of the more lightly damped resonance in the alloy shell. The feedback also effectively supresses the peaks in the scattered power due to the resonances of the $n = 3$ structural mode. For the alloy shell the result is that the scattered power has been reduced below that generated by a rigid sphere at all frequencies below about $ka = 6$.

A more selective approach to implementing the feedback controller is to make it modal [24], so that for the collocated case

$$\mathbf{H} = \mathbf{T}\ \mathbf{\Omega}\ \mathbf{T}^{\mathrm{H}}, \tag{48}$$

where $\mathbf{T}$ is the matrix of mode shapes at the transducer locations, and $\mathbf{\Omega}$ is a diagonal matrix of modal velocity feedback gains. Eq. (48) can then be substituted into Eq. (46) to give an expression for the structural impedance of the shell under modal control. In the limiting case, where it is assumed that there are as many actuators and sensors as there are significantly excited modes, then $\mathbf{T}$ is a square matrix and assuming that the transducers are positioned so as to actuate and sense all of the modes then $\mathbf{T}^{\mathrm{H}}\mathbf{T}$ is a good approximation to the identity matrix. Perfect control of all the modes is then possible, in principle, since the closed-loop impedance of the shell could be set equal to the input impedance of the volume of the scattering body filled with fluid, $\mathbf{Z}_I$, so that the scattering would be completely suppressed [6,7]. Setting Eq. (46) equal to $\mathbf{Z}_I$ in this case leads to a feedback controller having the form

$$\mathbf{H} = \mathbf{T}\ (\mathbf{Z}_I - \mathbf{Z}_B)\ \mathbf{T}^{\mathrm{H}}\ . \tag{49}$$

However, the performance of any feedback control system calculated in the frequency domain is dependant on the closed loop system being stable. Unfortunately, for the cases considered here, a feedback loop using the controller given by Eq. (49) was found to be unstable and so this frequency domain approach to calculating the modal controller is not helpful.

6. Non-axisymmetric excitation

In all the simulations above the primary and secondary excitation of the shell has been axisymmetric along the z axis, in which case only the $m = 0$ terms need to be included in the modal expansions for the pressure and velocity in Eqs. (11) and (12). This limits the number of elements required in the vectors of modal pressures and velocities to be $N+1$, rather than the more general $(N+1)^2$, and so greatly speeds up the calculation of the results. For an incident wave that is not propagating along the z axis, however, the more general formulation must be used, with all of the m and n terms in the modal series. If this more general simulation is performed for incident waves from other directions, with no active control, the results for the normalised scattered power from the uniform spherical shell are the same as those in Fig. 2. This is to be expected, since the scattered sound field is then just rotated to align with the incident field, but the overall scattered sound power is unaffected. Similarly, if the angular positions of the two actuators and sensors in Fig. 8 are adjusted to coincide with a modified angle of the incident wave, the results are the same as in Fig. 10. These results are as one would expect but do provide a good test that the formulation with both the n and m terms in the spherical harmonic expansion is working, and indeed that the spherical harmonic representation of the dynamics of the spherical shell is valid.

Of more interest is the case when using feedback control with actuators aligned along the z axis, but excited by a plane wave with the angles of incidence, θ_i and φ_i, which are different from zero. Fig. 11 shows the normalised scattered sound power with the two actuator/sensor arrangement used in Fig. 8 but for various different angles of incidence of the plane wave. The scales have been changed slightly compared with the figures above to make the results easier to see. In this case the matrix $\mathbf{Y}_B$ has 10,201 by 10,201 elements, in Eq. (10) for the scattered pressure, and so the calculations take considerably longer than in the axisymmetric case, where

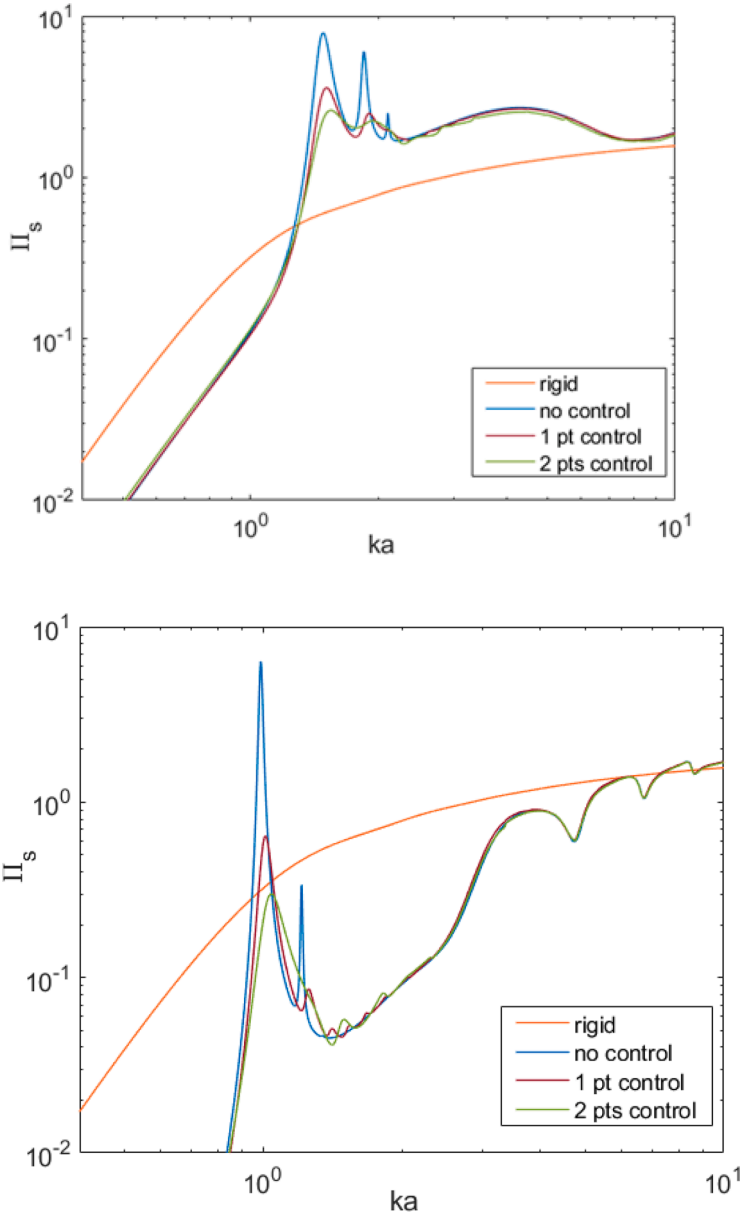

Fig. 10. Normalised scattered sound power from the steel shell, upper, and alloy shell, lower, after active feedback control with one or two spherical cap actuators and collocated velocity sensors, with $\theta_0 = \pi/10$, and decentralised velocoity feedback with a normalised gain of 0.2.

the dimensions of this matrix were only 101 by 101. It is clear from Fig. 10 that much less attenuation of the scattered power is achieved for the non-axisymmetric angles of incidence, reflecting the fact that the actuators aligned along the z axis are not able to effectively couple into the rotated structural mode shapes excited by the off-axis incident waves. In order to achieve levels of control that are less dependant on the angle of the incident wave it is necessary to use a larger number of actuators and sensors.

If 12 actuator/sensor pairs are used, for example, and these are placed at the vertices of a regular icosahedron, this also gives very poor attenuation of the scattered power for off-axis incident waves, since there are then rows of actuators on the latitudes of two of the nodal lines for some of the structural modes. Better results were obtained with 12 actuator/sensor pairs when the distribution was made less regular by offsetting the azimuthal position of these two rows of the regular icosahedron by 5° away from the poles, for which the results are shown in Fig. 12. This gives reasonable control of the $n = 2$ structural mode even for off-axis excitation. It may be possible to optimise the position of the actuator/sensor pairs for a particular set of incident angles, although this would be very time-consuming because of the computational issues discussed above, and would also be specific to the chosen set of incident angles. It would probably be better to reformulate the problem for diffuse field excitation and then optimise the actuator positions based on that more general form of excitation, but such a study is beyond the remit of the current paper.

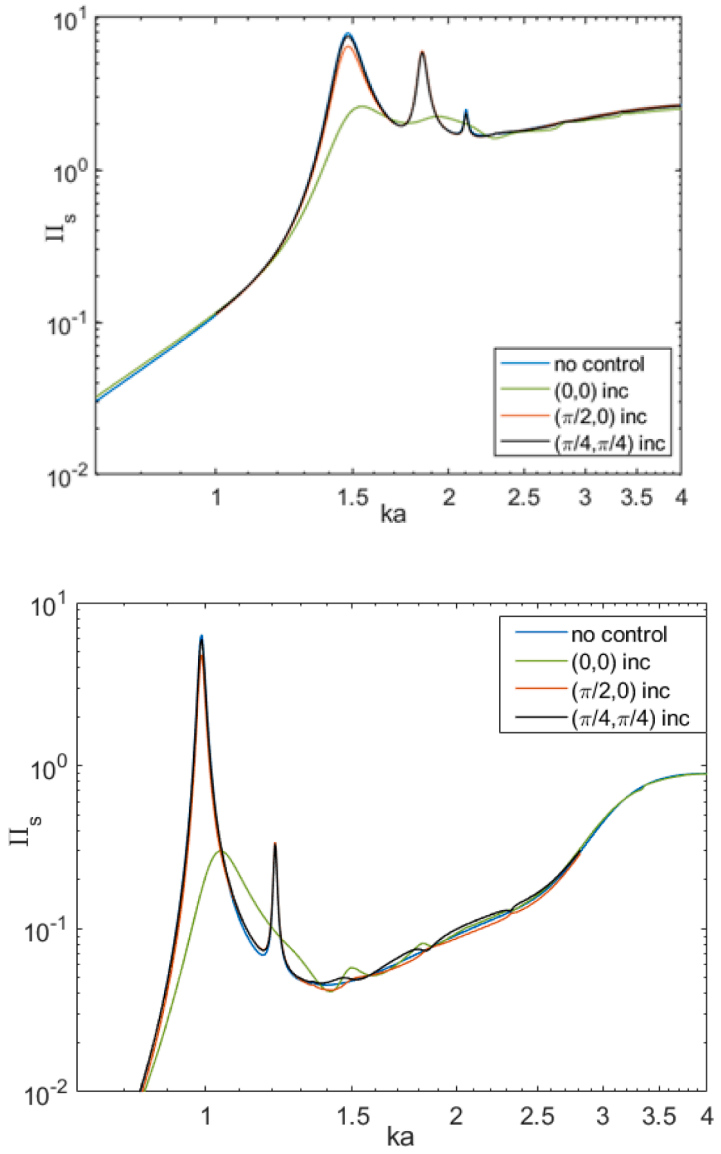

Fig. 11. Normalised scattered sound power from the steel shell, upper, and alloy shell, lower, after active feedback control with two spherical cap actuators and collocated velocity sensors using decentralised velocity feedback for different angles, $\boldsymbol{\theta}_i$ and $\boldsymbol{\varphi}_i$, of the incident plane wave. The results for $(\boldsymbol{\theta}_i, \boldsymbol{\varphi}_i) = (0,0)$ are the same as in Fig. 10 and are reproduced for reference. Note that for clarity the scales are slightly different from those used above.

7. Conclusions

A modal formulation for acoustic scattering from a flexible body is reviewed. This general theory is shown to take a particularly simple form in the case of scattering from a thin uniform empty spherical shell surrounded by an infinite fluid, since the internal and external acoustic modes, and the structural modes, are then all spherical harmonics. Examples of scattering are calculated for spherical shells of different materials. It is shown that the scattering due to both the structural breathing mode and the rigid body translational mode, which dominate at low frequencies, can be suppressed for an alloy shell with a suitable choice of the shell's material properties.

This formulation is then used to calculate the effect of active feedforward or feedback control on the scattering, initially using point force actuators on the flexible spherical shell. For feedback control, in order to effectively couple into the lower order structural modes that dominate the scattering it is found to be necessary to spread the actuation force over a distributed area, and to similarly average the measured velocity to maintain the duality of the collocated actuator/sensor pair. The effect of both feedforward and feedback control in reducing the scattering is mainly due to the suppression of a few lightly damped structural resonances. This is particularly effective on the alloy shell, for which several of the structural modes are lightly damped and contribute significantly to the scattered sound power at their resonant frequency. Although only two actuator/sensor pairs, on opposite sides of the shell, perform well in

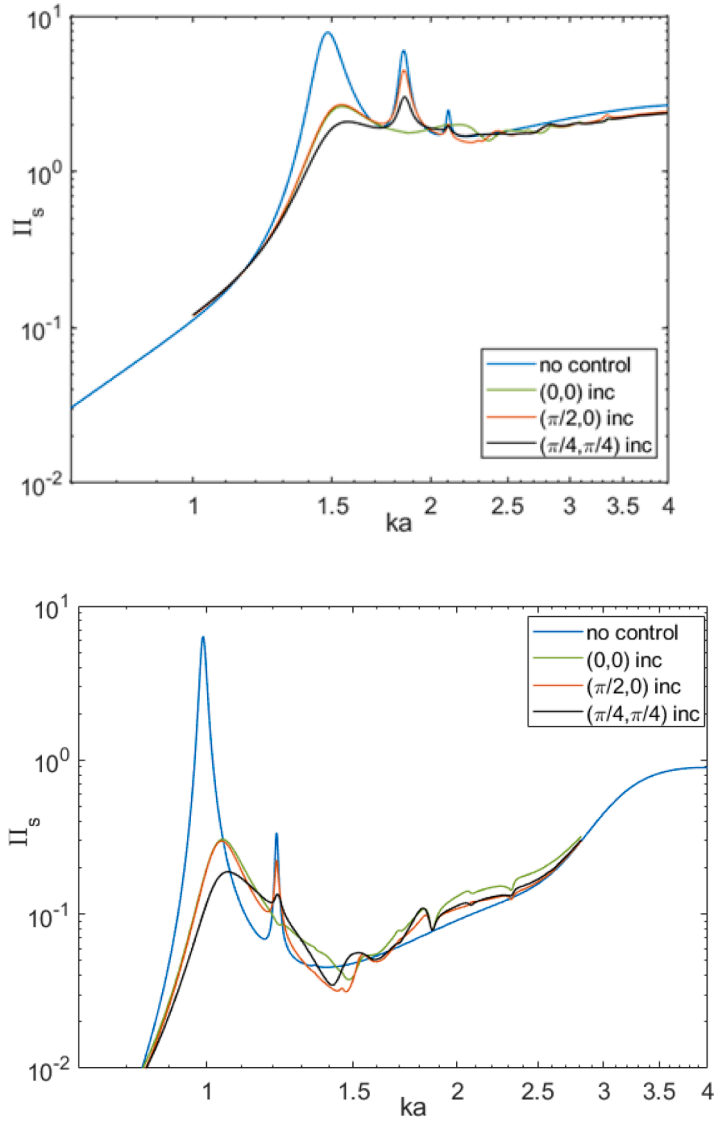

Fig. 12. Normalised scattered sound power from the steel shell, upper and alloy shell, lower, after active feedback control with twelve spherical cap actuators and collocated velocity sensors using decentralised velocity feedback, for the same incident angles (θ_i, φ_i) as in Fig. 11.

suppressing the scattering from incident waves along this axis, their performance is degraded for off-axis excitation. It is necessary to use a significantly larger number of actuator/sensor pairs to get reasonable control in this off-axis case, and the results are dependant on their orientation compared with the incident angle.

Although the numerical simulations have been based on an empty spherical shell, the general theoretical formulation is applicable to scattering bodies of arbitrary shape. The modal formulation in Section 2 can be applied to other, less symmetric, scattering bodies although the model expansion will then not, in general, diagonalise all of the three impedance matrices, so that some of these will be fully populated and the modal scattered pressure will not have such a simple analytic formulation. The principles of minimising the low frequency scattering in Section 3 are also applicable to other elastic bodies if their compressional stiffness and mass are known. In addition it is a general observation that at higher frequencies the scattering will be most significant at the resonant frequencies of the fluid-loaded elastic body [5]. If these resonances can be effectively damped using feedback control with structural actuators and sensors, then this strategy also has generally applicability as a method of reducing such scattering.

Authors contributions

Stephen Elliott originally conceived the structure of the paper and did most of the writing.
Mihai Orita did the original simulations and theoretical development.
Erika Quaranta simulated the final results and prepared most of the figures.

Jordan Cheer contributed to the theoretical development and structure of the paper.

Declaration of Competing Interest

The authors declare that they have no known competing financial interests or personal relationships that could have appeared to influence the work reported in this paper.

Data availability

No data was used for the research described in the article.

Acknowledgements

This work is supported by the Defence Science and Technology Laboratory, United Kingdom. We are grateful for discussions with Filippo Fazi in the preparation of Appendix B.

Appendix A. Derivation of equation (38)

By substituting Eq. (36) for p_{sc} into Eq. (37), the scattered power after control can be written as

$$W_{sc} = 2\pi a^2 \left[\mathbf{p}_s^{\mathrm{H}} - \widetilde{\mathbf{p}}_c^{\mathrm{H}}\mathbf{B}^{\mathrm{H}}\right] Re\{\mathbf{Y}_R\}[\mathbf{p}_s - \mathbf{B}\ \widetilde{\mathbf{p}}_c], \tag{A1}$$

Expressing this as

$$W_{sc} = 2\pi a^2 \left[\widetilde{\mathbf{p}}_c^{\mathrm{H}}\mathbf{B}^{\mathrm{H}} Re\{\mathbf{Y}_R\}\mathbf{B}\ \widetilde{\mathbf{p}}_c - \widetilde{\mathbf{p}}_c^{\mathrm{H}}\mathbf{B}^{\mathrm{H}} Re\{\mathbf{Y}_R\}\mathbf{p}_s - \mathbf{p}_s^{\mathrm{H}} Re\{\mathbf{Y}_R\}\mathbf{B}\ \widetilde{\mathbf{p}}_c + \mathbf{p}_s^{\mathrm{H}} Re\{\mathbf{Y}_R\}\mathbf{p}_s\right], \tag{A2}$$

it can be seen to be in the general Hermitian quadratic form of [2].

$$W_{sc} = 2\pi a^2 \left[\widetilde{\mathbf{p}}_c^{\mathrm{H}}\mathbf{A}\ \widetilde{\mathbf{p}}_c + \widetilde{\mathbf{p}}_c^{\mathrm{H}}\mathbf{b} + \mathbf{b}^{\mathrm{H}}\widetilde{\mathbf{p}}_c + c\right], \tag{A3}$$

where

$$\mathbf{A} = \mathbf{B}^{\mathrm{H}} Re\{\mathbf{Y}_R\}\mathbf{B}, \tag{A4}$$

$$\mathbf{b} = -\mathbf{B}^{\mathrm{H}} Re\{\mathbf{Y}_R\}\mathbf{p}_s, \tag{A5}$$

$$c = \mathbf{p}_s^{\mathrm{H}} Re\{\mathbf{Y}_R\}\mathbf{p}_s, \tag{A6}$$

Provided that the matrix $\mathbf{A}$ can be inverted, the general Hermitian quadratic form (A3) has a unique global minimum when $\widetilde{\mathbf{p}}_c$ is equal to $\widetilde{\mathbf{p}}_c^{(\mathrm{opt})} = -\mathbf{A}^{-1}\mathbf{b}$, which in this case is given by

$$\widetilde{\mathbf{p}}_c^{(\mathrm{opt})} = \left[\mathbf{B}^{\mathrm{H}} Re\{\mathbf{Y}_R\}\mathbf{B}\right]^{-1}\mathbf{B}^{\mathrm{H}} Re\{\mathbf{Y}_R\}\mathbf{p}_s. \tag{A7}$$

Using Eq. (10) then $\mathbf{p}_s$ can be expressed as $\mathbf{R}\ \mathbf{p}_i$ which leads to Eq. (38).

Appendix B. Coupling of spherical harmonics in a spherical cap

The purpose of this Appendix is to analyse the way in which the output of the spherical cap sensor is related to the spherical harmonic components of the surface velocity distribution on the shell, and hence derive Eq. (47). This is done by initially considering the axisymmetric case illustrated in Fig. 8, and then generalising the result for the case in which the sensor is centred on an arbitrary angle.

In general, the output of the distributed sensor, $\widetilde{v}_c$ can be written as

$$\widetilde{v}_c = \int_0^{\pi}\int_0^{2\pi} W(\theta,\varphi)\ V(\theta,\varphi)\ \sin\theta\ d\theta\ d\varphi \tag{B1}$$

where $V(\theta,\varphi)$ is the distribution of the complex velocity on the surface of the shell and $W(\theta,\varphi)$ is a spatial window function. The spatial window function can be expressed in terms of its spherical harmonic expansion, as was the surface velocity in Eq. (12), as

$$W(\theta,\varphi) = \sum_{n=0}^{\infty}\sum_{m=-n}^{n} w(n,m)\ Y_n^m(\theta,\varphi)\ . \tag{B2}$$

If the spatial window function is entirely real, this expansion is also equal to its conjugate, indicated again by an overbar. The

output of the sensor can then be written as

$$\widetilde{\mathrm{v}}_c = \sum_{n=0}^{\infty} \sum_{m=-n}^{n} \sum_{n'=0}^{\infty} \sum_{m'=-n'}^{n'} \overline{w}(n',m')\ v(n,m) \int_0^{\pi} \int_0^{2\pi} Y_n^m(\theta,\varphi)\ \overline{Y_{n'}^{m'}}(\theta,\varphi)\ \sin\theta d\theta d\varphi, \tag{B3}$$

and using the orthonormal properties of the spherical harmonics, this is equal to

$$\widetilde{\mathrm{v}}_c = \sum_{n=0}^{\infty} \sum_{m=-n}^{n} \overline{w}(n,m) v(n,m). \tag{B4}$$

In the axisymmetric case the spherical cap sensor that measures the spatially averaged velocity is centred on $\theta = 0$. The spatial window function in the interval $\theta = [0, \theta_0]$ is equal to $1/2\pi(1-\cos\theta_0)$, where the normalisation factor $2\pi(1-\cos\theta_0)$ is the solid angle subtended by the spherical cap, and the spatial window is zero otherwise. The spherical harmonic components of the window function can be calculated in general as

$$w(n,m) = \int_0^{\pi} \int_0^{2\pi} W(\theta,\varphi) \overline{Y_n^m}(\theta,\varphi)\ \sin\theta\ d\theta d\varphi \tag{B5}$$

where

$$\overline{Y_n^m}(\theta,\varphi) = \sqrt{\frac{(2n+1)(n-m)!}{4\pi(n+m)!}}\ P_n(\cos\theta) e^{-jm\varphi}. \tag{B6}$$

So that in the axisymmetric case, where $w(n,m)$ is equal to $w^0(n,m)$, say, this is given by

$$w^0(n,m) = \frac{1}{2\pi(1-\cos\theta_0)} \sqrt{\frac{2n+1}{4\pi}} \int_0^{\theta_0} P_n(\cos\theta)\sin\theta d\theta \int_0^{2\pi} \sqrt{\frac{(n-m)!}{(n+m)!}}\ e^{-jm\varphi} d\varphi. \tag{B7}$$

The integral over φ is equal to 2π if $m = 0$, but it is otherwise zero, and evaluating the integral of the Legendre polynomial [14], the spherical harmonic component in this axisymmetric case can be written as

$$w^0(n,0) = \frac{P_{n-1}(\cos\theta_0) - P_{n+1}(\cos\theta_0)}{(2n+1)(1-\cos\theta_0)} \sqrt{\frac{2n+1}{4\pi}}. \tag{B8}$$

This can be generalised to the case in which the sensor is centred on the angle $\varphi_k$and θ_k by first writing the spatial window in the axisymmetric case above as

$$W^0(\theta,\varphi) = \sum_{n=0}^{\infty} w^0(n,0)\ Y_n^0(\theta,\varphi) = \sum_{n=0}^{\infty} w^0(n,0)\ \sqrt{\frac{2n+1}{4\pi}}\ P_n(\cos\theta). \tag{B9}$$

If the sensor is now rotated to be centred on an angle of θ_k and φ_k, the spatial window function becomes

$$W(\theta,\varphi) = \sum_{n=0}^{\infty} w^0(n,m)\ \sqrt{\frac{2n+1}{4\pi}}\ P_n(\cos\Psi)\ , \tag{B10}$$

where Ψ is the angle between the evaluation point (θ,φ) and the centre of the sensor (θ_k,φ_k). Using the spherical harmonic summation formula [26],

$$\sum_{m=-n}^{n} Y_n^m(\theta,\varphi)\ \overline{Y_n^m}(\theta_k,\varphi_k) = \frac{2n+1}{4\pi}\ \ P_n(\cos\Psi). \tag{B11}$$

$W(\theta,\varphi)$ can then be written as

$$W(\theta,\varphi) = \sum_{n=0}^{\infty} w^0(n,m)\ \sqrt{\frac{4\pi}{2n+1}} \sum_{m=-n}^{n} Y_n^m(\theta,\varphi)\ \overline{Y_n^m}(\theta_k,\varphi_k), \tag{B12}$$

which is in the form of Eq. (B2) with

$$w(n,m) = w^0(n,m)\sqrt{\frac{4\pi}{2n+1}}\overline{Y_n^m}(\theta_k,\varphi_k) \tag{B13}$$

And using (B8) for $w^0(n,m)$

$$w(n,m) = \left[\frac{P_{n-1}(\cos\theta_0) - P_{n+1}(\cos\theta_0)}{(2n+1)(1-\cos\theta_0)}\right] \overline{Y_n^m}(\theta_k, \varphi_k) \tag{B14}$$

The output of a single sensor can be written using Eq. (42) as

$$\widetilde{v}_c = \sum_{n=0}^{\infty} \sum_{m=-n}^{n} T(n,m)\ v(n,m) \tag{B15}$$

Comparing this with Eq. (B4), it is seen that $T(n,m)$ is equal to $\overline{w}(n,m),$ so that Eq. (47) is given by

$$T(n,m) = \left[\frac{P_{n-1}(\cos\theta_0) - P_{n+1}(\cos\theta_0)}{(2n+1)(1-\cos\theta_0)}\right] Y_n^m(\theta_k, \varphi_k). \tag{B16}$$

In the limit where θ_0 becomes very small, the term in square brackets tends to unity, so this result is consistent with that used above for a point velocity sensor.

References

[1] W.L. Martens, R.O. Duda, Range dependence of the response of a spherical head model, J. Acoust. Soc. Am. 104 (5) (1998) 3048–4058.
[2] P.A. Nelson, S.J. Elliott, Active Control of Sound, Academic Press, London (UK), 1991.
[3] A.N. Norris, F.A. Amirkulava, W.J. Parnell, Source amplitudes for active exterior cloaking, Inverse Probl. 28 (2012), https://doi.org/10.1088/0266-5611/28/10/105002.
[4] W.S. Rayleigh, Investigation of the disturbance produced by a spherical obstacle on the waves of sound, in: Proceedings of the London Mathematical Society s1-4, 1871, pp. 253–283. Vols.
[5] M.C. Junger, D. Feit, Sound, Structures and Their Interactions, 2nd edition, MIT press, Maryland, Massachusetts, 1986.
[6] Y.I. Bobrovnitskii, A new impedance-based approach to analysis and control of sound scattering, J. Sound Vib. 297 (3–5) (2006) 743–760.
[7] Y.I. Bobrovnitskii, A new solution to the problem of an acoustical transparent body, Acoust. Phys. 50 (6) (2004) 647–650.
[8] D. Eggler, H. Chung, F. Montiel, J. Pan, N. Kessissoglou, Active noise cloaking of 2D cylindrical shells, Wave Motion 87 (2019) 106–122.
[9] S.J. Elliott, M. Orita, J. Cheer, A modal approach to acoustic scattering and its active control, in: Proc ICSV27, 2021.
[10] S.J. Elliott, M. Orita, Q. E, J. Cheer, Active control of acoustic scattering from a passively optimised spherical shell, in: Proc Internoise 2022, 2022.
[11] O.A. Godin, Rayleigh scattering of a spherical sound wave, J. Acoust. Soc. Am. 133 (2) (2013) 709–720.
[12] Y. Mao, J. Cai, Y. Gu, Q. D, Direct evaluation of acoustic-intensity, AIAA J. 53 (5) (2014) 1362–1371.
[13] S.J. Elliott, M. Orita, J. Cheer, Active control of the sound power scattered by a locally-reacting sphere, J. Acoust. Soc. Am. 147 (2020) 1851–1862.
[14] E.G. Williams, Fourier Acoustics: Sound Radiation and Nearfield Acoustical Holography, 1999, p. 1999. London (UK).
[15] W.E. Baker, Axisymmetric modes of vibration of thin spherical shells, J. Acoust. Soc. Am. 33 (1961) 1749–1758.
[16] M. Orita, Control of 3D Sound Scattering based on Decomposition into Spherical Harmonic Components, PhD thesis, University of Southampton, 2021.
[17] A. Alu, N. Engheta, Achieving transparency with plasmonic and metamaterials coatings, Phys. Rev. E 72 (1) (2005) 16623.
[18] M.D. Guild, A. Alu, M.R. Haberman, Cancellation of acoustic scattering from an elastic sphere, J. Acoust. Soc. Am. 129 (3) (2011) 1355–1365.
[19] A.C. Rohde, et al., Experimental demonstration of underwater acoustic scattering cancellation, Sci. Rep. 5 (3) (2015) 13175.
[20] H. Lamb, The Dynamical Theory of Sound, Dover Publications, New York, 1960.
[21] E. Friot, C. Bordier, Real-time active suppression of scattered acoustic radiation, J. Sound Vib. 278 (2004) 563–580.
[22] S.J. Elliott, Signal Processing for Active Control, Academic press, London (UK), 2001.
[23] E.J. Avital, E.J. Miloh, Sound scattering and its cancellation by an elastic spherical shell in free space and near a free surface, Wave Motion 55 (2015) 35–47.
[24] A. Preumont, Vibration Control of Active Structures: An Introduction, 3rd Edition, Kluwer Academic Publishers, Dordrecht, 1999.
[25] S.J. Elliott, P. Gardonio, C.T. Sors, M.J. Brennan, Active control with multiple local feedback loops, J. Acoust. Soc. Am. 111 (2) (2002) 908–915.
[26] [Online]. Available: https://functions.wolfram.com/Polynomials/SphericalHarmonicY/23/ShowAll.html.